

Scalarized Einstein-Born-Infeld-scalar Black Holes

Peng Wang,^{*} Houwen Wu,[†] and Haitang Yang[‡]

Center for Theoretical Physics, College of Physics,

Sichuan University, Chengdu, 610064, China

Abstract

The phenomenon of spontaneous scalarization of Reissner-Nordström (RN) black holes has recently been found in an Einstein-Maxwell-scalar (EMS) model due to a non-minimal coupling between the scalar and Maxwell fields. Non-linear electrodynamics, e.g., Born-Infeld (BI) electrodynamics, generalizes Maxwell's theory in the strong field regime. Non-minimally coupling the BI field to the scalar field, we study spontaneous scalarization of an Einstein-Born-Infeld-scalar (EBIS) model in this paper. It shows that there are two types of scalarized black hole solutions, i.e., scalarized RN-like and Schwarzschild-like solutions. Although the behavior of scalarized RN-like solutions in the EBIS model is quite similar to that of scalarized solutions in the EMS model, we find that there exist significant differences between scalarized Schwarzschild-like solutions in the EBIS model and scalarized solutions in the EMS model. In particular, the domain of existence of scalarized Schwarzschild-like solutions possesses a certain region, which is composed of two branches. The branch of larger horizon area is a family of disconnected scalarized solutions, which do not bifurcate from scalar-free black holes. However, the branch of smaller horizon area may or may not bifurcate from scalar-free black holes depending on the parameters. Additionally, these two branches of scalarized solutions can be both entropically disfavored over comparable scalar-free black holes in some parameter region.

^{*}Electronic address: pengw@scu.edu.cn

[†]Electronic address: iverwu@scu.edu.cn

[‡]Electronic address: hyanga@scu.edu.cn

Contents

I. Introduction	2
II. EBIS Model	4
III. Born-Infeld Black Hole	8
IV. Scalarized Born-Infeld Black Hole	10
A. Scalarized RN-like Born-Infeld Black Hole	12
B. Scalarized Schwarzschild-like Born-Infeld Black Hole	13
V. Discussion and Conclusion	18
Acknowledgments	21
References	21

I. INTRODUCTION

Recent observations of gravitational waves [1] and the black-hole shadow [2] have provided us with a better understanding of black hole nature in the strong gravity regime. Specially, these observations have opened up a new era to test the no-hair theorem [3–6], which is crucial to understand black hole physics. The no-hair theorem states that a black hole is uniquely characterized by three observable properties, its mass, angular momentum and electrical charge. Testing the no-hair theorem in experiments can help us constrain alternative theories of gravity, which often contain extra scalar fields. On the other hand, black holes can become a new venue for the detection of the scalar fields themselves [7, 8]. Although the no-hair theorem has been proven for a number of field-theory models (e.g., the Einstein-Maxwell theory), various counter-examples were found. The first counter-example is hairy black hole solutions in the context of the Einstein-Yang-Mills theory [9–11]. Later, black hole solutions with Skyrme hairs [12, 13] and dilaton hairs [14] were obtained. For a review, see [15].

To understand the formation of hairy black holes, the phenomenon of spontaneous scalarization was discussed for neutron stars in scalar-tensor models [16]. In this phenomenon,

the non-minimal coupling of the scalar field to the Ricci curvature can lead to a certain parameter region, where scalar-free and scalarized neutron star solutions coexist, and the scalarized solution is energetically favoured. Later on, spontaneous scalarization was generalized to black holes in scalar-tensor models [17, 18]. Recently, spontaneous scalarization has been realized in the extended Scalar-Tensor-Gauss-Bonnet (eSTGB) gravity, in which the scalar field is non-minimally coupled to Gauss-Bonnet curvature corrections of the gravitational sector [19–24]. However in the eSTGB models, studying dynamical evolution is challenging due to non-linear curvature terms in the evolution equations. Subsequently, a simpler type of model, namely the Einstein-Maxwell-scalar (EMS) models, was introduced to gain a deeper insight into spontaneous scalarization [25]. In the EMS models, spontaneous scalarization can be triggered by the strong non-minimal coupling of the scalar field to the electromagnetic field. A massless and non-self-interacting scalar field was considered in [25], where an exponential coupling function was introduced to ensure a tachyonic instability of Reissner-Nordström (RN) black holes. Shortly afterwards, spontaneous scalarization in the EMS models was further discussed in context of coupling functions beyond the exponential coupling [26, 27], dyons including magnetic charges [28], axionic-type couplings [29], massive and self-interacting scalar fields [30, 31], horizonless reflecting stars [32], linear stability of scalarized black holes [33–35], higher dimensional scenario [36], quasinormal modes of scalarized black holes [37, 38], two U(1) fields [39], and quasi-topological electromagnetism [40]. Analytic approximations were also used to study spontaneous scalarization of the EMS models [41–43].

Non-linear electrodynamics (NLED) is an effective model incorporating quantum corrections to Maxwell’s electromagnetic theory. In the Einstein-NLED theories, various NLED charged black holes were derived and discussed in a number of papers [44–51]. Among various NLED, there is a famous string-inspired one: Born-Infeld (BI) electrodynamics, which encodes the low-energy dynamics of D-branes. BI electrodynamics was first proposed to smooth divergences of the electrostatic self-energy of point charges by introducing a cutoff on electric fields [52]. After BI black hole solutions were obtained [53, 54], their properties have been extensively investigated in the literature [55–67].

One of the motivations for this work is to understand the effect of NLED corrections on the EMS models. Specifically, we numerically obtain and study scalarized black hole solutions in the Einstein-Born-Infeld-scalar (EBIS) model with an exponential coupling.

The rest of this paper is organized as follows. Section II presents the basics of the EBIS model and provides the equations of motion for the solution ansatz of interest. In section III, we discuss various properties of scalar-free BI black hole solutions. Section IV contains our main numerical results for scalarized black hole solutions, which include domains of existence, thermodynamic preference and effective potentials for radial perturbations. We summarize our results with a brief discussion in section V.

II. EBIS MODEL

We consider a real scalar field ϕ minimally coupled to Einstein's gravity and non-minimally coupled to the BI electromagnetic field A_μ , which is described by the action

$$S = \int d^4x \sqrt{-g} \left[R - 2\partial_\mu \phi \partial^\mu \phi + \frac{4f(\phi)}{a} \left(1 - \sqrt{1 + aF^{\mu\nu}F_{\mu\nu}/2} \right) \right]. \quad (1)$$

Here we take $16\pi G = 1$ for simplicity, the coupling parameter a is related to the string tension α' as $a = (2\pi\alpha')^2 > 0$, $F_{\mu\nu} = \partial_\mu A_\nu - \partial_\nu A_\mu$ is the BI electromagnetic field strength tensor, and $f(\phi)$ is the coupling function governing the non-minimal coupling of ϕ and A_μ . When $a \rightarrow 0$, we can recover the EMS model from the action (1). The equations of motion that follow from the action (1) are

$$\begin{aligned} R_{\mu\nu} - \frac{1}{2}Rg_{\mu\nu} &= \frac{\mathcal{T}_{\mu\nu}}{2}, \\ \partial_\mu \left[\frac{\sqrt{-g}f(\phi)F^{\mu\nu}}{\sqrt{1 + aF^{\mu\nu}F_{\mu\nu}/2}} \right] &= 0, \\ \frac{\partial^\mu (\sqrt{-g}\partial_\mu \phi)}{\sqrt{-g}} &= -\dot{f}(\phi) \frac{1 - \sqrt{1 + aF^{\mu\nu}F_{\mu\nu}/2}}{a}, \end{aligned} \quad (2)$$

where $\dot{f}(\phi) \equiv df(\phi)/d\phi$, and the energy-momentum tensor is given by

$$\mathcal{T}_{\mu\nu} = 4 \left(\partial_\mu \phi \partial_\nu \phi - \frac{g_{\mu\nu} \partial_\rho \phi \partial^\rho \phi}{2} \right) + 4f(\phi) \left[\frac{1 - \sqrt{1 + aF^{\mu\nu}F_{\mu\nu}/2}}{a} g_{\mu\nu} + \frac{F_{\mu\rho}F_\nu{}^\rho}{\sqrt{1 + aF^{\mu\nu}F_{\mu\nu}/2}} \right]. \quad (3)$$

The generic spherically symmetric metric can be written as

$$ds^2 = -N(r) e^{-2\delta(r)} dt^2 + \frac{dr^2}{N(r)} + r^2 (d\theta^2 + \sin^2 \theta d\varphi^2), \quad (4)$$

where we introduce the Misner-Sharp mass function $m(r)$ as in $N(r) = 1 - 2m(r)/r$. Due to the spherical symmetry, the electromagnetic field and the scalar field are given by

$A_\mu dx^\mu = V(r) dt$ and $\phi = \phi(r)$, respectively. With this ansatz, the equations of motion (2) then reduce to

$$\begin{aligned}
N'(r) - \frac{1}{r} [1 - N(r)] + r\phi'(r)^2 N(r) &= \frac{2}{aQ^2} \left[r^2 f(\phi) - \sqrt{aQ^2 + f^2(\phi) r^4} \right], \\
[r^2 N(r) \phi'(r)]' + r^3 \phi'(r)^3 N(r) &= -\frac{Q^2 r^2 \dot{f}(\phi)}{aQ^2 + f^2(\phi) r^4 + f(\phi) r^2 \sqrt{aQ^2 + f^2(\phi) r^4}}, \\
\delta'(r) &= -r\phi'(r)^2 \\
V'(r) &= -\frac{e^{-\delta(r)} Q}{\sqrt{aQ^2 + f^2(\phi) r^4}},
\end{aligned} \tag{5}$$

where primes denote derivatives with respect to the radial coordinate r , and Q is a constant that can be interpreted as the electric charge.

To find asymptotically flat black hole solutions of the non-linear ordinary differential equations (5), one needs to impose regular boundary conditions at the event horizon and spatial infinity. The regularity of the solutions across the event horizon at $r = r_+$ gives that the solutions can be approximated by a power series expansion in $r - r_+$,

$$\begin{aligned}
m(r) &= \frac{r_+}{2} + (r - r_+) m_1 + \dots, \quad \delta(r) = \delta_0 + (r - r_+) \delta_1 + \dots, \\
\phi(r) &= \phi_0 + (r - r_+) \phi_1 + \dots, \quad V(r) = (r - r_+) v_1 + \dots
\end{aligned} \tag{6}$$

where

$$\begin{aligned}
m_1 &= \frac{2\sqrt{aQ^2 + f^2(\phi_0)r_+^4} - 2f(\phi_0)r_+^2}{2a}, \\
\delta_1 &= \frac{Q^4 \dot{f}^2(\phi_0) r_+^3 \left\{ 4 [a + 2f(\phi_0)r_+^2] \left[\sqrt{aQ^2 + f^2(\phi_0)r_+^4} + f(\phi_0)r_+^2 \right] + a(a + 4Q^2) \right\}}{[a + 4f(\phi_0)r_+^2 - 4Q^2]^2 \left\{ r_+^2 f(\phi_0) \left[\sqrt{aQ^2 + f^2(\phi_0)r_+^4} + f(\phi_0)r_+^2 \right] + aQ^2 \right\}^2}, \\
\phi_1 &= -\frac{r_+ \dot{f}(\phi_0) \left[\sqrt{aQ^2 + f^2(\phi_0)r_+^4} - r_+^2 f(\phi_0) + 2Q^2 \right]}{[a + 4r_+^2 f(\phi_0) - 4Q^2] \sqrt{aQ^2 + f^2(\phi_0)r_+^4}}, \\
v_1 &= -\frac{e^{-\delta_0} Q}{\sqrt{aQ^2 + f^2(\phi_0)r_+^4}}.
\end{aligned} \tag{7}$$

The two parameters, ϕ_0 and δ_0 , determine the expansion coefficients and hence the solutions in the vicinity of the horizon. The Hawking temperature T_H and the horizon area A_H are given by

$$T_H = \frac{N'(r_+) e^{-\delta(r_+)}}{4\pi} \quad \text{and} \quad A_H = 4\pi r_+^2, \tag{8}$$

respectively. At spatial infinity, the asymptotic expansion of the solutions takes the form,

$$m(r) = M - \frac{Q^2 + Q_s^2}{2r} + \dots, \delta(r) = \frac{Q_s^2}{2r^2} + \dots, \phi(r) = \frac{Q_s}{r} + \frac{Q_s M}{r^2} + \dots, V(r) = \Phi + \frac{Q}{r}, \quad (9)$$

where we assume $f(0) = 1$. Here M is the the ADM mass, Φ is the electrostatic potential measured at infinity, and Q_s is the scalar charge. With the asymptotic behavior of the solutions at $r = r_+$ and $r = \infty$, we can use a standard shooting method to solve eqn. (5) for a family of black hole solutions. Note that the solutions and the associated physical quantities scale as

$$r \rightarrow \lambda r, \phi \rightarrow \phi, m \rightarrow \lambda m, V \rightarrow V, \delta \rightarrow \delta, Q \rightarrow \lambda Q, M \rightarrow \lambda M, a \rightarrow \lambda^2 a, \quad (10)$$

where λ is a constant. For later use, we then introduce some reduced quantities,

$$q = \frac{Q}{M}, \tilde{a} = \frac{a}{Q^2}, a_H = \frac{A_H}{16\pi M^2}, t_H = 8\pi M T_H, \quad (11)$$

which are dimensionless and invariant under the scaling symmetry (10).

The Smarr relation [68] relates the black hole mass to other physical quantities, and can be used to test the accuracy of numerical black hole solutions. For a manifold \mathcal{M} endowed with the time-like Killing vector K^μ , we consider a hypersurface Σ with the boundary $\partial\Sigma$. Due to Gauss's law and Einstein's equations, integrating the identity for Killing vectors $\nabla_\mu (\nabla_\nu K^\mu) = K^\mu R_{\mu\nu}$ over the hypersurface Σ yields

$$\int_{\partial\Sigma} dS_{\mu\nu} \nabla^\mu K^\nu = \frac{1}{2} \int_\Sigma dS_\mu K_\nu \left(\mathcal{T}^{\mu\nu} - \frac{1}{2} \mathcal{T} g^{\mu\nu} \right), \quad (12)$$

where $dS_{\mu\nu}$ is the surface element on $\partial\Sigma$, dS_μ denotes the volume element on Σ , and $\mathcal{T}^{\mu\nu}$ is the stress-energy tensor. For the metric (4), the Killing vector $K^\mu = (1, 0, 0, 0)$, and we choose the hypersurface of constant time t bounded by the horizon and spatial infinity to be Σ , such that the boundary $\partial\Sigma$ consists of $r = r_+$ and $r = +\infty$. Using eqns. (3) and (5), we find that the Smarr relation is given by

$$M = 2\pi r_+^2 T_H + Q\Phi + \int_{r_+}^{\infty} \frac{Q^2 e^{-\delta(r)}}{\sqrt{\tilde{a}Q^4 + f^2(\phi)r^4}} \left[\frac{2f(\phi)r^2}{\sqrt{\tilde{a}Q^4 + f^2(\phi)r^4 + f(\phi)r^2}} - 1 \right] dr, \quad (13)$$

where the last term vanishes for the EMS model with $a = 0$.

To study perturbative stability of black hole solutions, one can consider spherically symmetric and time-dependent linear perturbations around the black hole (4). The metric ansatz including the perturbations can be written as [26]

$$ds^2 = -\tilde{N}(r, t) e^{-2\tilde{\delta}(r, t)} dt^2 + \frac{dr^2}{\tilde{N}(r, t)} + r^2 (d\theta^2 + \sin^2 \theta d\varphi^2), \quad (14)$$

where

$$\tilde{N}(r, t) = N(r) + \epsilon \tilde{N}_1(r) e^{-i\Omega t} \text{ and } \tilde{\delta}(r, t) = \delta(r) + \epsilon \tilde{\delta}_1(r) e^{-i\Omega t}. \quad (15)$$

The time dependence of the perturbations is assumed to be Fourier modes with frequency Ω . Similarly for the scalar and BI fields, the ansatz is given by

$$\tilde{\phi}(r, t) = \phi(r) + \epsilon \tilde{\phi}_1(r) e^{-i\Omega t} \text{ and } \tilde{V}(r, t) = V(r) + \epsilon \tilde{V}_1(r) e^{-i\Omega t}, \quad (16)$$

respectively. Plugging the ansatzes (15) and (16) into the equations of motion (2), we find that the gravity equations lead to

$$\tilde{\delta}_1(r) = -2r\phi'(r)\tilde{\phi}'_1(r), \quad \tilde{N}_1(r) = -2rN(r)\phi'(r)\tilde{\phi}_1(r), \quad (17)$$

and the BI field equation gives

$$\tilde{V}'_1(r) = -V'(r) \left\{ \tilde{\phi}_1(r) \frac{\dot{f}(\phi)}{f(\phi)} [1 - ae^{2\delta(r)}V'(r)^2] + \tilde{\delta}_1(r) f(\phi) \right\}. \quad (18)$$

With the help of eqns. (5), (17) and (18), we can express the perturbation equation for $\tilde{\phi}_1(r)$ in the familiar Schrödinger-equation form,

$$-\frac{d^2\Phi}{dr^{*2}} + U_\Omega\Phi = \Omega^2\Phi, \quad (19)$$

where $\Phi \equiv r\tilde{\phi}_1(r)$, and r^* is the tortoise coordinate defined by $dr^*/dr = e^{\delta(r)}N^{-1}(r)$. The effective potential U_Ω is

$$U_\Omega = \frac{N(r)e^{-2\delta(r)}}{r^2} \left\{ 1 - N(r) - 2r^2\phi'(r)^2 + \frac{Q^2}{\sqrt{\tilde{a}Q^4 + f^2(\phi)r^4}} \left[\frac{\dot{f}^2(\phi)r^4}{\tilde{a}Q^4 + f^2(\phi)r^4} - 2 + 4r^2\phi'(r)^2 \right] \right. \\ \left. + \frac{r^2}{a} \left(\frac{f(\phi)r^2}{\sqrt{\tilde{a}Q^4 + f^2(\phi)r^4}} - 1 \right) \left[4r\phi'(r)\dot{f}(\phi) + 2f(\phi)(2r^2\phi'(r)^2 - 1) + \ddot{f}(\phi) \right] \right\}, \quad (20)$$

which can be shown to vanish at the event horizon and spatial infinity via the asymptotic expansions (6) and (9). An unstable mode of the EBIS model that has $\Omega^2 < 0$ would then correspond to a bound state of U_Ω . From quantum mechanics, it follows that if the bound state exists, Ω^2 must exceed the minimum value of U_Ω . Therefore, when U_Ω is always positive for $r \in (r_+, +\infty)$, no bound states exist, and hence the black hole solutions are stable against spherically symmetric perturbations. However, note that the appearance of a negative region in U_Ω does not necessarily mean the presence of radial instability [30]. In this case, one may need other methods, such as the S-deformation method [69], to investigate the stability of the solutions.

III. BORN-INFELD BLACK HOLE

In this paper, we study spontaneous scalarization of the EBIS model, which requires a scalar-free solution. The existence of such a solution then leads to $\dot{f}(0) = 0$, which is obtained via the scalar equation in eqn. (2). In this section, we consider the scalar-free solution to eqn. (5) with $\dot{f}(0) = 0$. When the scalar field $\phi = 0$, the static spherically symmetric black hole solution was first derived in [53, 54],

$$N(r) = 1 - \frac{2M}{r} - \frac{2Q^2}{3\sqrt{r^4 + \tilde{a}Q^4} + 3r^2} + \frac{4Q^2}{3r^2} {}_2F_1\left(\frac{1}{4}, \frac{1}{2}, \frac{5}{4}; -\frac{\tilde{a}Q^4}{r^4}\right),$$

$$\delta(r) = 0 \text{ and } V'(r) = -\frac{Q}{\sqrt{r^4 + \tilde{a}Q^4}}, \quad (21)$$

where M and Q are the mass and charge of the black hole, respectively. The Hawking temperature of the BI black hole can be calculated from eqn. (8):

$$T_H = \frac{1}{4\pi r_+} \left(1 - \frac{2Q^2}{r_+^2 + \sqrt{r_+^4 + \tilde{a}Q^4}} \right), \quad (22)$$

where r_+ is the horizon radius. It showed in [63] that there are two types of BI black holes depending on the minimum value of T_H :

- RN type: $\tilde{a} \leq 4$. This type of BI black holes can have extremal black hole solutions like RN black holes. For $T_H = 0$, the horizon radius of the extremal BI black hole is $r_e \equiv Q\sqrt{1 - \tilde{a}/4}$. We plot T_H versus r_+ for a RN-like BI black hole with $\tilde{a} = 3$ in the left panel of FIG. 1, where we have $Q = 1$, and the black hole becomes extremal at $r_e = 1/2$. Similar to a RN black hole, the mass-to-charge ratio of a RN-like BI black hole reaches the maximum when the black hole is extremal. The right panel of FIG. 1 shows the maximum mass-to-charge ratio q_{\max} versus \tilde{a} for RN-like BI black holes, which is represented by a red line.
- Schwarzschild-like type: $\tilde{a} > 4$. Like Schwarzschild black holes, the Hawking temperature T_H of this type of BI black holes is always greater than zero, and diverges as $r_+ \rightarrow 0$. We display T_H against r_+ for a Schwarzschild-like BI black hole with $\tilde{a} = 10$ and $Q = 1$ in the left panel of FIG. 1, which shows that T_H is a monotonically decreasing function of r_+ , and becomes infinite at $r_+ = 0$. Unlike the RN case, the largest mass-to-charge ratio q_{\max} occurs when $r_+ = 0$ with Q being finite. The BI

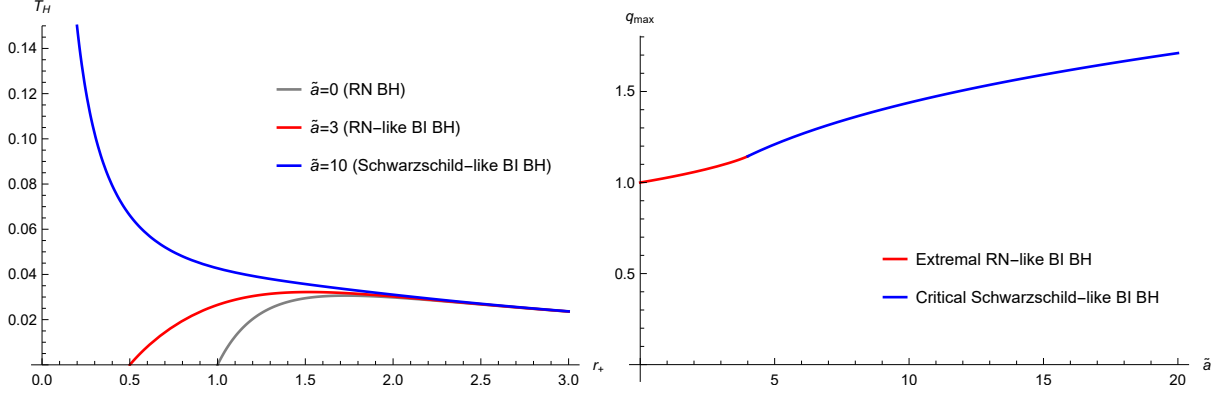


FIG. 1: **Left:** Plot of the Hawking temperature T_H against the horizon radius r_+ for a RN black hole with $\tilde{a} = 0$, a RN-like BI black hole with $\tilde{a} = 3$ and a Schwarzschild-like BI black hole with $\tilde{a} = 10$. Here we take $Q = 1$. For $\tilde{a} = 0$ and $\tilde{a} = 3$, the black holes possess an extremal limit, where $T_H = 0$. For $\tilde{a} = 10$, the black hole temperature behaves like that of a Schwarzschild black hole, in that it approaches infinity as r_+ goes to zero. **Right:** Plot of the maximum value of the mass-to-charge ratio q_{\max} against \tilde{a} . Extremal RN-like BI black holes have the largest mass-to-charge ratio, while q_{\max} occurs at critical Schwarzschild-like BI black holes, which have $r_+ = 0$ while Q remains finite.

black holes that have vanishing r_+ and finite Q (or M) are dubbed as critical BI black holes. In the right panel of FIG. 1, q_{\max} versus \tilde{a} for Schwarzschild-like BI black holes is depicted by a blue line.

To study the stability of the BI black hole solution against a scalar perturbation $\delta\phi$, we linearize the scalar equation in eqn. (2) around the scalar-free solution, which gives

$$\frac{\partial^\mu (\sqrt{-g} \partial_\mu \delta\phi)}{\sqrt{-g}} = \mu_{eff}^2 \text{ with } \mu_{eff}^2 = -\ddot{f}(0) \frac{1 - r^2/\sqrt{r^4 + \tilde{a}Q^4}}{aQ^2}. \quad (23)$$

If $\mu_{eff}^2 < 0$, a tachyonic instability is induced, and a scalarized black hole solution can bifurcate from the scalar-free BI black hole solution. Note that $\mu_{eff}^2 < 0$ leads to $\ddot{f}(0) > 0$. In the remainder of the paper, we focus an exponential coupling, $f(\phi) = e^{\alpha\phi^2}$ with $\alpha > 0$, which satisfies $\dot{f}(0) = 0$ and $\ddot{f}(0) > 0$.

To study the onset of spontaneous scalarization from the scalar-free solution, we derive the zero mode of BI black holes. First, we express the scalar perturbation $\delta\phi$ as a spherical harmonics decomposition

$$\delta\phi = \sum_{l,m} Y_{lm}(\theta, \phi) U_l(r). \quad (24)$$

With this decomposition, the scalar equation (23) then simplifies to

$$\frac{\partial_r [r^2 N(r) U_l'(r)]}{r^2} - \left[\frac{l(l+1)}{r^2} + \mu_{eff}^2 \right] U_l(r) = 0, \quad (25)$$

where $N(r)$ is given by eqn. (21). In addition, $U_l(r)$ is regular at $r = r_+$ and vanishes at $r = \infty$. With fixed α and l , the boundary conditions of $U_l(r)$ would pick up a set of BI black hole solutions with different reduced charge q . The black hole solutions can be labelled by a non-negative integer n , and $n = 0$ is the fundamental mode, whereas $n > 0$ corresponds to overtones. In this paper, we focus on the $l = 0 = n$ mode since it gives the smallest q of the black hole solutions for a given α [25]. The reduced charge $q_{\text{exist}}(\alpha)$ of the $l = 0 = n$ mode compose the bifurcation line in the α - q plane, on which scalarized black hole solutions emerge from the BI black holes. In the upper left panel of FIG. 2, the blue dashed line represents the bifurcation line of a RN-like BI black hole with $\tilde{a} = 3$, which is quite similar to the RN black hole case [25]. The bifurcation line of a Schwarzschild-like BI black hole with $\tilde{a} = 10$ is shown by a blue dashed line (hardly distinguished from the cyan line for large α) in FIG. 3. When α is large, the bifurcation lines in the RN- and Schwarzschild-like cases are almost same. Interestingly for small α , the bifurcation line in the Schwarzschild-like case bears little resemblance to that in the RN-like case. Specifically, the right panel of FIG. 3 shows that Schwarzschild-like BI black holes with $\tilde{a} = 10$ and $\alpha \in (2.846, 3.139)$ have two $l = 0 = n$ modes, which marks the onset of two families of scalarized black hole solutions.

IV. SCALARIZED BORN-INFELD BLACK HOLE

In this section, we present the numerical results, e.g., domains of existence, thermodynamic preference and effective potentials, for scalarized black hole solutions, which are dynamically induced from RN-like BI black holes with $\tilde{a} = 3$ and Schwarzschild-like BI black holes with $\tilde{a} = 10$. To solve the non-linear differential equations (5) for the scalarized black hole solutions, we express the differential equations (5) in terms of a new coordinate

$$x = 1 - \frac{r_+}{r} \text{ with } 0 \leq x \leq 1, \quad (26)$$

and employ the NDSolve function in Wolfram Mathematica to numerically solve the equations in the interval $10^{-8} \leq x \leq 1$. Solving the differential equations (5) numerically is quite standard except possible stiffness encountered around $x = 1$. So we use the ‘‘StiffnessSwitching’’ method, which by default switches between the backward differentiation formula and

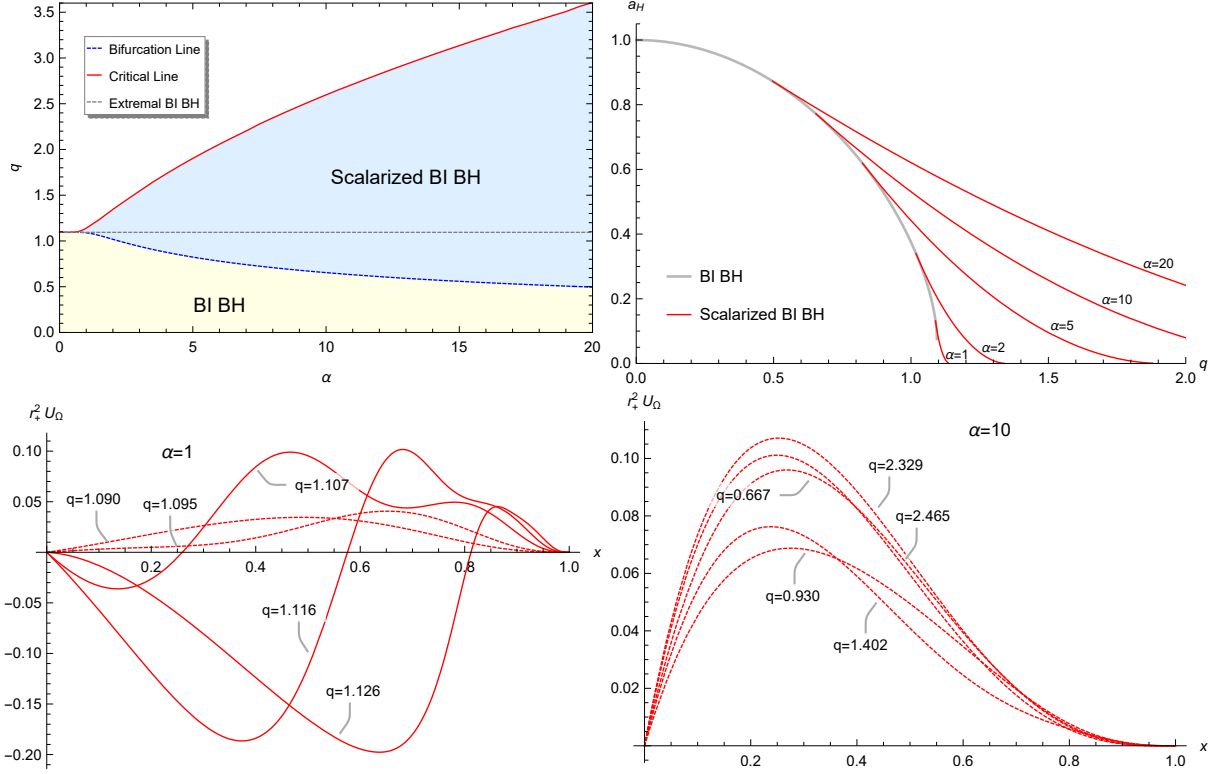


FIG. 2: Domain of existence, thermodynamic preference and effective potentials for scalarized RN-like BI black hole solutions with $\tilde{a} = 3$. **Upper Left:** Domain of existence in the α - q plane, which is displayed by a shaded light blue region and bounded by the bifurcation and critical lines. The blue dashed line represents the bifurcation line, where scalarized black holes bifurcate from BI black holes as zero modes. The red line marks critical configurations of scalarized black holes, where the horizon area vanishes with the mass remaining finite. In the light blue region, only one branch of scalarized black hole solutions exists for a given α . **Upper Right:** Reduced area a_H versus reduced charge q for BI black holes (a gray line) and scalarized BI black holes with various values of α (red lines). For a given q , a_H of the scalarized BI black hole is larger than that of the BI black hole, and increases with the growth of α . The scalarized solutions are always entropically preferred. **Lower:** Effective potentials for scalarized BI black holes with $\alpha = 1$ (**Left**) and $\alpha = 10$ (**Right**) for various values of q . Dashed red lines represent positive definite effective potentials, whereas effective potentials that have negative regions are exhibited by solid red lines. The $\alpha = 10$ scalarized solutions are stable against radial perturbations, while the stability of the $\alpha = 1$ scalarized solutions is inconclusive.

Adams methods, depending on whether the system being solved is stiff or not. To test the accuracy of the numerical method, we consider the Smarr relation (13), and our numerical results exhibit that the numerical error can be maintained around the order of 10^{-6} . In what follows, we confine ourselves to the simplest case of nodeless, spherically symmetric black hole solutions and leave general configurations for future work.

A. Scalarized RN-like Born-Infeld Black Hole

In the upper left panel of FIG. 2, we present the domain of existence for scalarized RN-like BI black holes with $\tilde{a} = 3$. For a given α , scalarized solutions emerge from the bifurcation line as zero modes, and can be continuously induced by increasing q until they reach the critical line. Our numerical results suggest that, for scalarized solutions on the critical line, the horizon radius r_+ vanishes, whereas the mass M and the charge Q remain finite. The domain of existence for scalarized solutions is bounded by the bifurcation and critical lines, and shows a close resemblance to that of RN black holes [25]. For given α and q in the domain of existence, the numerics show that there exists a unique set of nodeless scalarized solutions. We plot the reduced area a_H of the scalarized solutions against the reduced charge q for several values of α in the upper right panel of FIG. 2, which indicates that scalarized solutions are entropically preferred over BI black hole solutions.

To study stability of scalarized solutions, we depict effective potentials for scalarized solutions with $\alpha = 1$ and $\alpha = 10$ in the lower row of FIG. 2. When $\alpha = 1$, the scalarized solutions have positive effective potentials for small enough value of q , and thus are free of radial instabilities. However, as q increases, negative regions in the effective potentials appear, and hence radial instabilities cannot be excluded. Moreover, the negative regions of the potentials becomes larger when moving toward the critical line, i.e., for larger q . On the other hand, the effective potentials of the scalarized solutions with $\alpha = 10$ are shown to be positive, which indicates that the scalarized solutions are radially stable. Note that solid and dashed colored lines, which represent effective potentials in the following figures, correspond to potentials with and without negative regions, respectively.

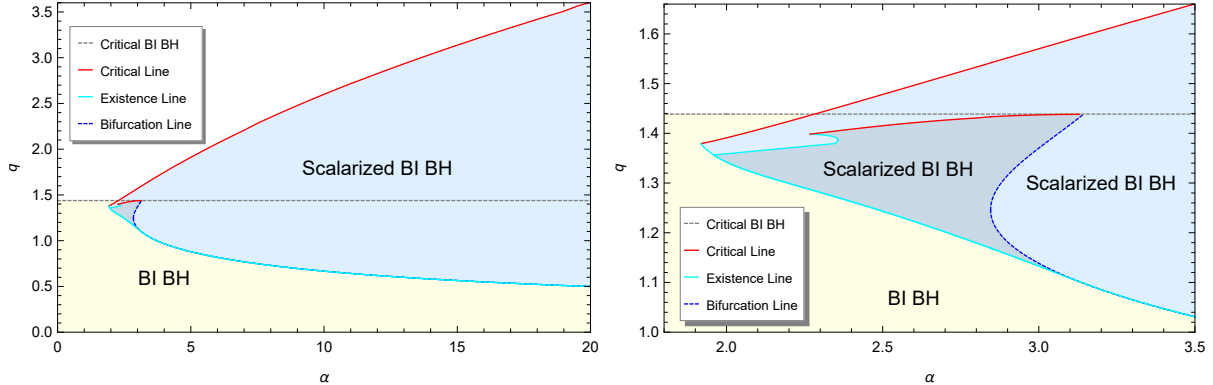


FIG. 3: Domain of existence for scalarized Schwarzschild-like BI black hole solutions with $\tilde{a} = 10$. For a given α , scalarized black hole solutions possess two branches in the dark shaded blue region and one branch in the light one. The domain of existence is delimited by the critical (red lines) and existence (cyan lines) lines. While scalarized solutions emerge with vanishing scalar fields on the bifurcation line (a blue dashed line), scalarized solutions on the existence lines have non-vanishing scalar field configurations. When α is large, the bifurcation and existence lines are hardly distinguishable from each other, and the domain of existence is quite similar to that in the $\tilde{a} = 3$ case. The right panel headlights the small α region, where the domains of existence in the RN-like and Schwarzschild-like cases are significantly different.

B. Scalarized Schwarzschild-like Born-Infeld Black Hole

The domain of existence in the α - q plane for scalarized Schwarzschild-like BI black holes with $\tilde{a} = 10$ is displayed in FIG. 3, where the right panel highlights small α regime. Apart from the existence and critical lines, which appear in the RN-like case, a new type of boundaries of the domain of existence, dubbed as “existence line”, is present in the Schwarzschild-like case. Unlike the bifurcation line, scalarized solutions on the existence line are not zero modes, and have non-zero finite scalar field (except $x = 1$). The domain of existence for scalarized solutions with $\tilde{a} = 10$ is bounded by the existence, bifurcation and critical lines, and have more complicated structure than the RN-like case. As q varies, scalarized solutions in the dark blue regions of FIG. 3 have two α -constant branches, while these in the light blue regions have only one α -constant branch.

When α is large enough, our numerical results barely discriminate between the existence and bifurcation lines. Practically for a given a , scalarized black holes start from the bifurcation (existence) lines, and form the single branch of solutions with monotonically increasing

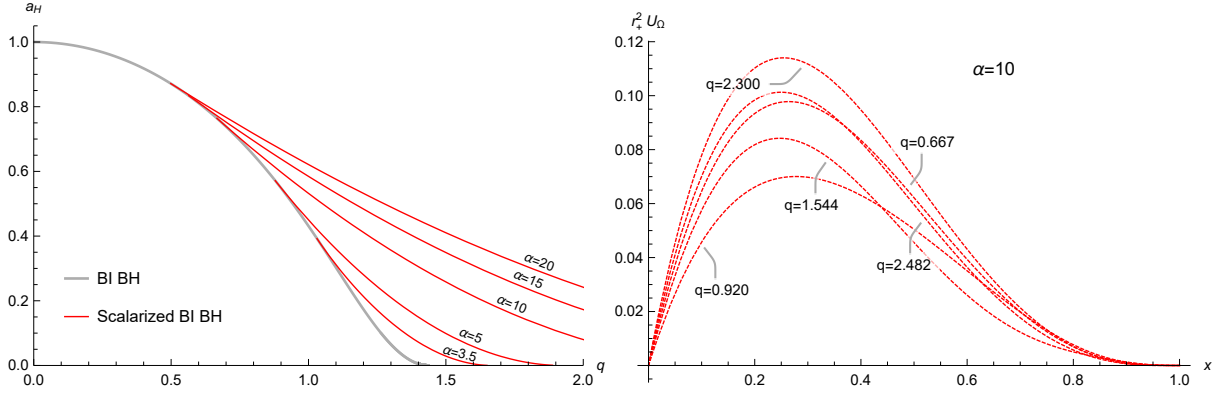


FIG. 4: Thermodynamic preference and effective potentials for Schwarzschild-like BI black hole solutions with $\tilde{a} = 10$ in the large α regime. **Left:** Reduced area a_H versus reduced charge q for BI black holes (a gray line) and scalarized BI black holes with various values of $\alpha \geq 3.5$ (red lines). The scalarized solutions are always entropically preferred. **Right:** Effective potentials for scalarized solutions with $\alpha = 10$ for various values of q , which are shown to be positive. The scalarized BI black hole solutions are stable against radial perturbations.

q until the critical line is reached. We plot the reduced area a_H against the reduced charge q for scalarized solutions with several values of α in the left panel of FIG. 4, which displays that the scalarized solutions have larger area than BI black holes, and hence are entropically preferred. Effective potentials of scalarized solutions with $\alpha = 10$ are presented for various values of q in the right panel of FIG. 4. It exhibits that the effective potentials are positive, and hence the scalarized solutions are stable against radial perturbations. Our results suggest that, in large α regime, the behavior of scalarized RN-like and Schwarzschild-like black hole solutions is quite alike.

For $2.846 \lesssim \alpha \lesssim 3.138$, we observe from the right panel of FIG. 3 that the bifurcation (blue dashed) line is multi-valued for a given α , i.e., two reduced charges, $q_{\text{bi}}^{\text{up}}(\alpha)$ and $q_{\text{bi}}^{\text{low}}(\alpha)$ with $q_{\text{bi}}^{\text{up}}(\alpha) > q_{\text{bi}}^{\text{low}}(\alpha)$, correspond to a same α on the bifurcation line. The scalarized black holes with $q_{\text{bi}}^{\text{up}}(\alpha)$ and $q_{\text{bi}}^{\text{low}}(\alpha)$ give rise to three branches of scalarized solutions, namely large branch, small branch and tiny branch, in the domain of existence. With increasing q , the tiny branch emerges from the scalarized black holes with $q_{\text{bi}}^{\text{up}}(\alpha)$ on the bifurcation line, and ends at a singular configuration with $q_{\text{cr}}^{\text{low}}(\alpha)$ on the red lower critical line in FIG. 3. The tiny branch then exists for $q_{\text{bi}}^{\text{up}}(\alpha) \leq q \leq q_{\text{cr}}^{\text{low}}(\alpha)$. The small branch starts from zero modes with

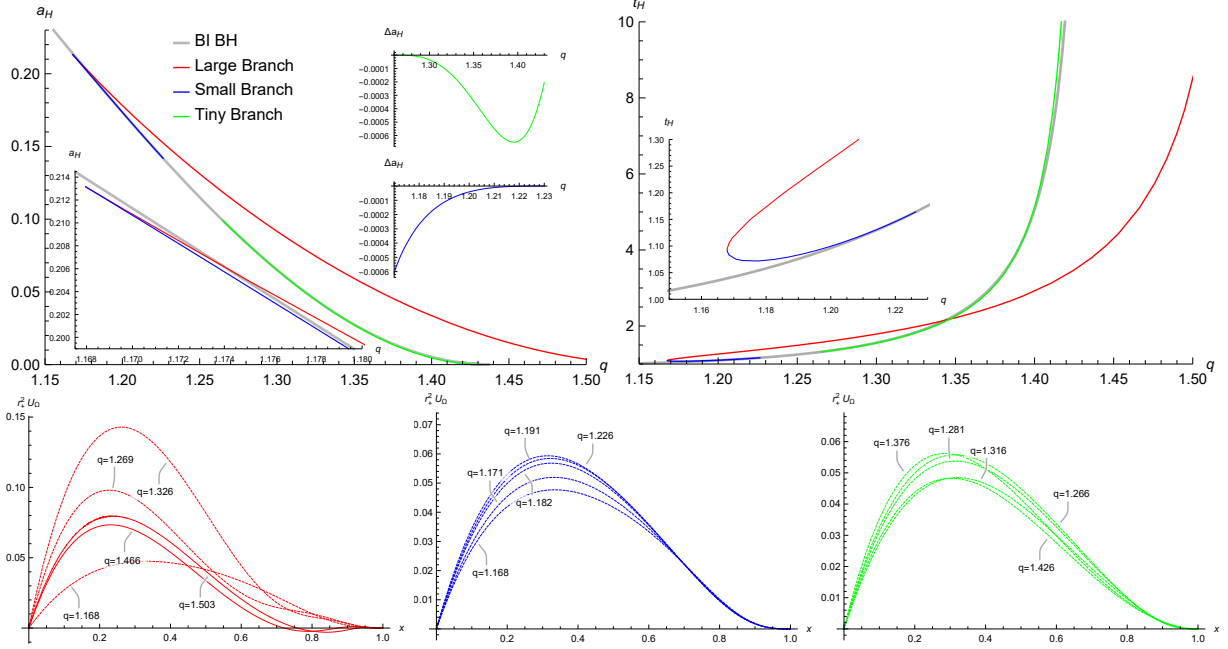


FIG. 5: Thermodynamic preference, temperature and effective potentials for the large (red lines), small (blue lines) and tiny (green lines) branches of Schwarzschild-like BI black hole solutions with $\tilde{a} = 10$ and $\alpha = 2.85$. The large branch coexists with the small and tiny branches, respectively. **Upper Left:** Reduced area a_H versus reduced charge q for BI black holes (a gray line) and the three branches of scalarized BI black holes. The difference of the reduced areas of the scalarized and BI black holes $\Delta a_H \equiv a_H^{\text{scalarized BH}} - a_H^{\text{BI BH}}$ is plotted against q for the small and tiny branches in the insets on the right of the panel, which show that the small and tiny branches have smaller area than BI black holes for same q . The inset on the left side displays that most of the large branch is entropically preferred. **Upper Right:** Reduced temperature t_H versus reduced charge q for BI black holes and the three branches of scalarized BI black holes. For a given q , the large branch is hotter than the small branch, while large branch is colder than the tiny branch when q is large enough. **Lower:** Effective potentials for the three branches of scalarized BI black holes with various values of q . The small and tiny branches are stable against radial perturbations. When q is small, the large branch is also stable. However for large q , the stability of the large branch is inconclusive.

$q_{\text{bi}}^{\text{low}}(\alpha)$ on the bifurcation line and have a decreasing reduced charge q until a minimum value, $q_{\text{ex}}(\alpha)$, is achieved. The curve $q_{\text{ex}}(\alpha)$ is the cyan existence line in FIG. 3. On the existence line, the scalarized solutions bifurcates, and a new branch of solutions, i.e., the large branch, appears. As q increases from $q_{\text{ex}}(\alpha)$, the large branch reaches out into the region beyond

the existence of BI black holes and terminates at the the upper critical line with $q_{\text{cr}}^{\text{upp}}(\alpha)$. The large and small branches exist for $q_{\text{ex}}(\alpha) \leq q \leq q_{\text{cr}}^{\text{upp}}(\alpha)$ and $q_{\text{ex}}(\alpha) \leq q \leq q_{\text{bi}}^{\text{low}}(\alpha)$, respectively. Since $q_{\text{ex}}(\alpha) < q_{\text{bi}}^{\text{low}}(\alpha)$ and $q_{\text{bi}}^{\text{up}}(\alpha) < q_{\text{cr}}^{\text{low}}(\alpha) < q_{\text{cr}}^{\text{upp}}(\alpha)$, the large branch coexists with the small (tiny) branch when $q_{\text{ex}}(\alpha) \leq q \leq q_{\text{bi}}^{\text{low}}(\alpha)$ ($q_{\text{bi}}^{\text{up}}(\alpha) \leq q \leq q_{\text{cr}}^{\text{low}}(\alpha)$).

To illustrate the properties of the three branches, we plot the reduced area a_H against the reduced charge q , the reduced temperature t_H against the reduced charge q and effective potentials for the three branches with $\alpha = 2.85$ in FIG. 5. The insets in the upper left panel of FIG. 5 show that the small and tiny branches always have smaller area (entropy) than the BI black holes with the same q . However except the small part around the existence line, most of the large branch have larger area and hence is entropically preferred. In addition, the upper left panel of FIG. 5 indicates that the large (tiny) branch has the largest (smallest) area, which justifies the terms, large, small and tiny, for the three branches. The reduced temperature t_H against the reduced charge q is depicted for the three branches and BI black holes in the upper right panel of FIG. 5. All the temperatures monotonically increase as q increases. In the coexistence region, the large branch is hotter than the small branch, whereas both branches are hotter than BI black holes. There is a crossing of t_H of the large and tiny branches between $q_{\text{ex}}^{\text{up}}(\alpha)$ and $q_{\text{cr}}^{\text{low}}(\alpha)$. For large (small) q , the large branch is colder (hotter) than the tiny branch and BI black holes. The effective potentials for the three branches are presented for several q in the lower row of FIG. 5, which shows that the small branch, the tiny branch and the part of the large branch that is far enough away from the critical line are radially stable. For q close enough to $q_{\text{cr}}^{\text{upp}}(\alpha)$, the effective potentials of the large branch have negative regions, which occurs away from the horizon. So the analysis of radial stability is inconclusive in this case.

When $1.959 \lesssim \alpha \lesssim 2.846$, the bifurcation line ceases to exist, and two branches of scalarized black holes, namely large branch and small branch, would emerge and bifurcate from the existence line with the minimum q of the domain of existence. The large branch is the reminiscent of the large branch in the $2.846 \lesssim \alpha \lesssim 3.138$ case, and also ends at the upper critical line. On the other hand, the small branch is the reminiscent of the small and tiny branches in the $2.846 \lesssim \alpha \lesssim 3.138$ case, and terminates at the lower critical line or other existence line. To better understand the two branch structure of the scalarized solutions, we will consider scalarized solutions with $\alpha = 2.5$ and 2.2 .

In FIG. 6, we plot a_H versus q , t_H versus q and effective potentials for scalarized black

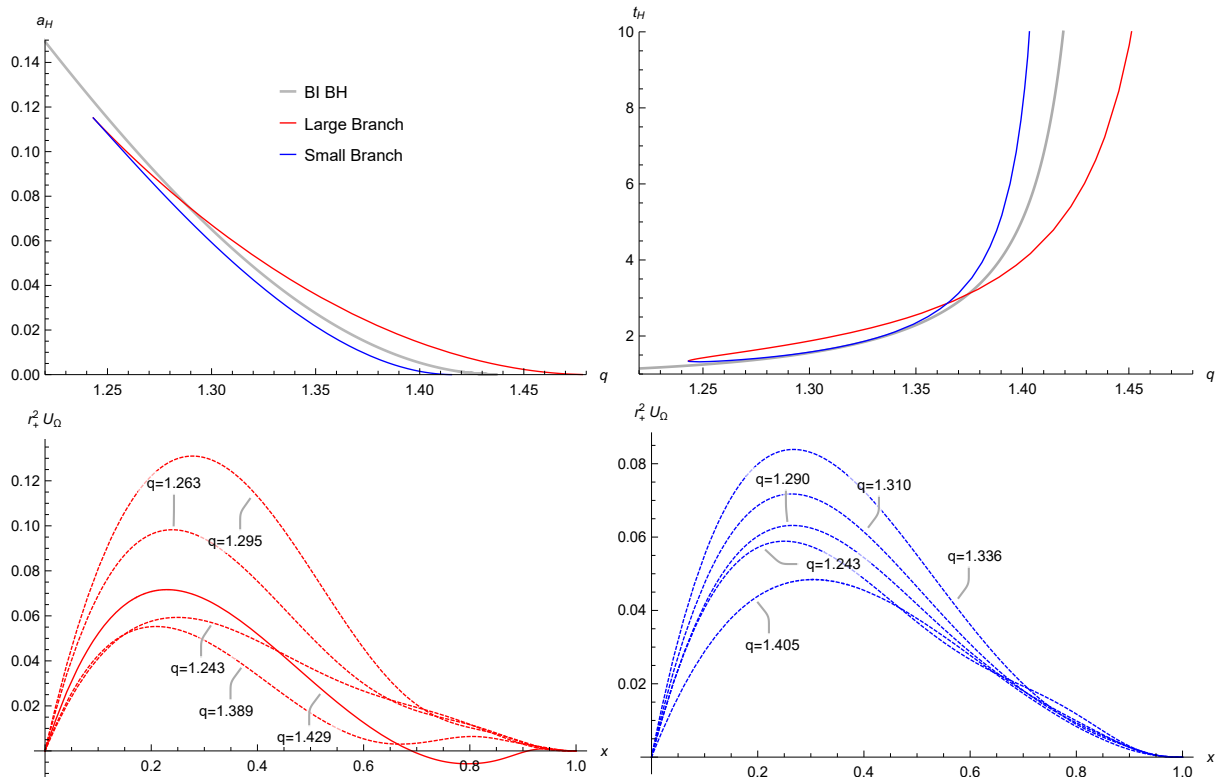


FIG. 6: Thermodynamic preference, temperature and effective potentials for the large (red lines) and small (blue lines) branches of Schwarzschild-like BI black hole solutions with $\tilde{a} = 10$ and $\alpha = 2.5$. **Upper Left:** Reduced area a_H versus reduced charge q for BI black holes (a gray line) and the two branches of scalarized BI black holes. For a given q , the small branch and the part of the large branch with small q have smaller area than BI black holes. When q is large enough, the large branch is entropically preferred. **Upper Right:** Reduced temperature t_H versus reduced charge q for BI black holes and the two branches of scalarized BI black holes. The large branch is hotter (colder) than the small branch for small (large) values of q . **Lower:** Effective potentials for the two branches of scalarized BI black holes with various values of q . The small branch and the large branch with small q are stable against radial perturbations. However for large q , the stability of the large branch is inconclusive.

hole solutions with $\alpha = 2.5$. The upper left panel justifies the terms for the large and small branches, since it shows that the reduced area of the large branch is larger than that of the small branch. The upper left panel also displays that the end configurations of the two branches possess vanishing horizon area, corresponding to the critical lines. In comparison with BI black holes, the small branch also has smaller area. As q increases from

the existence line toward the critical line, the reduced area of the large branch is initially less and then becomes greater than that of BI black holes with the same q . So the large branch is entropically preferred when q is large enough. Interestingly, the part of the large branch that is entropically disfavored becomes larger in the $\alpha = 2.5$ case than in the $\alpha = 2.85$ case. The upper right panel of FIG. 6 exhibits that the temperatures of the two branches are monotonically increasing functions of q . Additionally, as q grows, the large branch is first colder and then becomes hotter than the small branch. In the lower row of FIG. 6, we present effective potentials for the two branches for several values of q . Near the critical line, the effective potential of the large branch owns a negative part, which means stability is inconclusive. However for the small branch and the part of the large branch at a distance from the critical line, the effective potentials are positive, which suggests that they are radially stable.

In FIG. 7, we present a_H versus q , t_H versus q and effective potentials for scalarized black hole solutions with $\alpha = 2.2$. According to the left upper panel, the large and small branches end at the critical and some existence lines, respectively. Moreover, it shows that the two branches are entropically disfavored since they have smaller area than BI black holes with the same q . From the upper right panel, one observes that, except small part of the small branch near the end configuration, the temperature of the large branch is higher than that of the small branch. Effective potentials for the two branches are plotted in the lower row of FIG. 7, which indicates that the two branches can be stable against radial perturbations when q is small enough.

V. DISCUSSION AND CONCLUSION

In this paper, we studied scalarized black hole solutions in the EBIS model with the non-minimal coupling function $f(\phi) = e^{\alpha\phi^2}$, which is subclass IIA according to the classification suggested in [28]. In subclass IIA, scalar-free solutions suffer from a tachyonic instability, and scalarized solutions can bifurcate from the scalar-free solutions on bifurcation lines, which consists of zero modes of the scalar-free solutions. In the EBIS model, scalar-free solutions are BI black holes given in eqn. (21), which have been shown to possess two types of solutions, i.e., RN-like and Schwarzschild-like BI black holes. In the α - q plane, bifurcation lines of RN-like BI and RN black holes are very similar (see FIG. 2), whereas bifurcation

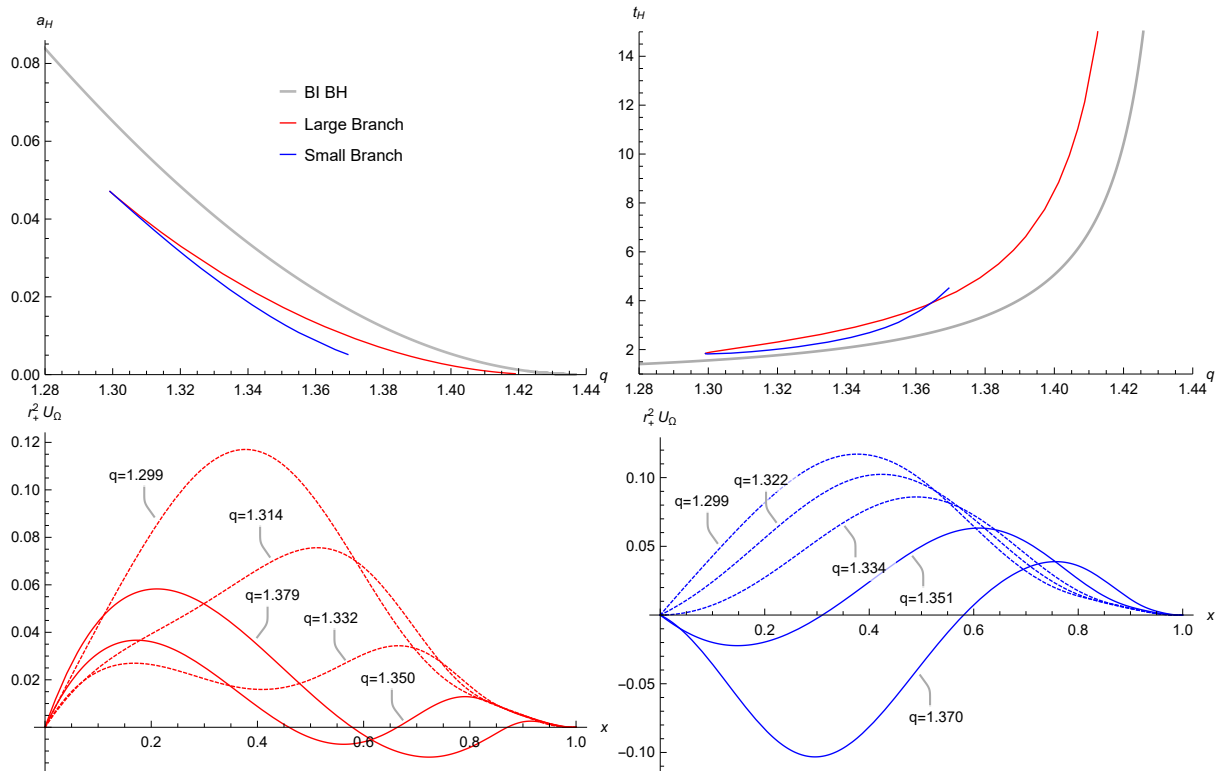


FIG. 7: Thermodynamic preference, temperature and effective potentials for the large (red lines) and small (blue lines) branches of Schwarzschild-like BI black hole solutions with $\tilde{a} = 10$ and $\alpha = 2.25$. **Upper Left:** Reduced area a_H versus reduced charge q for BI black holes (a gray line) and the two branches of scalarized BI black holes. For a given q , the small and large branches both have smaller area than BI black holes, which means that the scalarized solutions are not entropically preferred. **Upper Right:** Reduced temperature t_H versus reduced charge q for BI black holes and the two branches of scalarized BI black holes. The scalarized solutions are hotter than BI black holes, and the large branch is hotter (colder) than the small branch for small (large) values of q . **Lower:** Effective potentials for the two branches of scalarized BI black holes with various values of q . When q is large, the stability of the scalarized solutions is inconclusive. For small enough q , the scalarized solutions are stable against radial perturbations.

lines of Schwarzschild-like BI and RN black holes have quite different behavior in small α regime (see FIG. 3). Specifically, the bifurcation line of Schwarzschild-like BI black holes is a double-valued function of α in some region of the parameter space.

To gain insight into scalarized solutions, the domains of existence, thermodynamic preference, radial stability and temperature of these solutions were numerically investigated for the

RN-like case with $\tilde{a} = 3$ and the Schwarzschild-like case with $\tilde{a} = 10$, respectively. For the scalarized RN-like black hole solutions, the domain of existence is bounded by the existence and critical lines, which resembles the EMS models very closely (see FIG. 2). Moreover, we found that the scalarized RN-like black hole solutions have only one branch, which is always entropically preferred over the BI black holes with the same q , and almost radially stable except for the parameter region close to the critical line in the small α regime (see FIG. 2). These observations imply that the scalarized solutions are candidate endpoints of the evolution of unstable RN-like BI black holes.

On the other hand, the domain of existence for the scalarized Schwarzschild-like black hole solutions is different with the existence of a new type of boundary, where scalarized solutions with a non-trivial scalar field profile exist, and a new parameter region, where two branches of solutions coexist (see FIG. 3). When α is large enough, the scalarized solutions have been shown to be entropically favoured over comparable BI black holes and stable against radial perturbations (see FIG. 4). In some small α regime, scalarized solutions have three branches, which are named as the large, small and tiny branches, respectively, according to the black hole reduced areas (see FIG. 5). The small and tiny branches bifurcate from zero modes of BI black holes, whereas the large branch does not connect with BI black holes. Except small parameter region near the existence line, the large branch of the solutions is always entropically favoured over the small and tiny branches and comparable BI black holes. In addition, the large branch is radially stable in the parameter region far away enough from the critical line. Further decreasing α , we found the small and tiny branches can join together to form a new small branch of solutions, which becomes disconnected from BI black holes (see FIG. 6). The large branch is entropically favoured over comparable BI black holes when it is far away enough from the existence line. The parameter region that the large branch is entropically disfavoured grows as α decreases. The large branch is also radially stable when it is at a distance from the critical line. Finally, there exists some smaller α , for which BI black holes are entropically favoured over the large and small branches of scalarized solutions (see FIG. 7).

In this paper, we have presented preliminary results of the EBIS model with the exponential coupling and observed that effects of NLED can play a significant role in certain parameters. Let us conclude with some comments regarding potential future research directions. It would be interesting to study excited scalarized solutions since only the fundamental state

was considered in this paper. For the EMS model, it has been shown that the fundamental state is entropically preferred over excited states [25]. Apart from the exponential coupling, studying other coupling functions, e.g., a subclass IIB quartic coupling function, can reveal new phenomena. Richer structure, e.g., hot and cold branches, have been observed in the EMS model of subclass IIB [27]. Finally, obtaining rotating scalarized BI black holes and fully non-linear evolutions of the EBIS model are always desirable.

Acknowledgments

We are grateful to Shuxuan Ying and Zhipeng Zhang for useful discussions and valuable comments. This work is supported in part by NSFC (Grant No. 11875196, 11375121, 11947225 and 11005016).

-
- [1] B.P. Abbott et al. Observation of Gravitational Waves from a Binary Black Hole Merger. *Phys. Rev. Lett.*, 116(6):061102, 2016. [arXiv:1602.03837](#), [doi:10.1103/PhysRevLett.116.061102](#).
 - [2] Kazunori Akiyama et al. First M87 Event Horizon Telescope Results. I. The Shadow of the Supermassive Black Hole. *Astrophys. J.*, 875(1):L1, 2019. [arXiv:1906.11238](#), [doi:10.3847/2041-8213/ab0ec7](#).
 - [3] Werner Israel. Event horizons in static vacuum space-times. *Phys. Rev.*, 164:1776–1779, 1967. [doi:10.1103/PhysRev.164.1776](#).
 - [4] B. Carter. Axisymmetric Black Hole Has Only Two Degrees of Freedom. *Phys. Rev. Lett.*, 26:331–333, 1971. [doi:10.1103/PhysRevLett.26.331](#).
 - [5] Remo Ruffini and John A. Wheeler. Introducing the black hole. *Phys. Today*, 24(1):30, 1971. [doi:10.1063/1.3022513](#).
 - [6] Mohsen Khodadi, Alireza Allahyari, Sunny Vagnozzi, and David F. Mota. Black holes with scalar hair in light of the Event Horizon Telescope. *JCAP*, 09:026, 2020. [arXiv:2005.05992](#), [doi:10.1088/1475-7516/2020/09/026](#).
 - [7] Richard Brito, Vitor Cardoso, and Paolo Pani. *Superradiance: New Frontiers in Black Hole Physics*, volume 906. Springer, 2015. [arXiv:1501.06570](#), [doi:10.1007/978-3-319-19000-6](#).

- [8] Yifan Chen, Jing Shu, Xiao Xue, Qiang Yuan, and Yue Zhao. Probing Axions with Event Horizon Telescope Polarimetric Measurements. *Phys. Rev. Lett.*, 124(6):061102, 2020. [arXiv:1905.02213](#), [doi:10.1103/PhysRevLett.124.061102](#).
- [9] M.S. Volkov and D.V. Galtsov. NonAbelian Einstein Yang-Mills black holes. *JETP Lett.*, 50:346–350, 1989.
- [10] P. Bizon. Colored black holes. *Phys. Rev. Lett.*, 64:2844–2847, 1990. [doi:10.1103/PhysRevLett.64.2844](#).
- [11] Brian R. Greene, Samir D. Mathur, and Christopher M. O’Neill. Eluding the no hair conjecture: Black holes in spontaneously broken gauge theories. *Phys. Rev. D*, 47:2242–2259, 1993. [arXiv:hep-th/9211007](#), [doi:10.1103/PhysRevD.47.2242](#).
- [12] Hugh Luckock and Ian Moss. BLACK HOLES HAVE SKYRMION HAIR. *Phys. Lett. B*, 176:341–345, 1986. [doi:10.1016/0370-2693\(86\)90175-9](#).
- [13] Serge Droz, Markus Heusler, and Norbert Straumann. New black hole solutions with hair. *Phys. Lett. B*, 268:371–376, 1991. [doi:10.1016/0370-2693\(91\)91592-J](#).
- [14] P. Kanti, N.E. Mavromatos, J. Rizos, K. Tamvakis, and E. Winstanley. Dilatonic black holes in higher curvature string gravity. *Phys. Rev. D*, 54:5049–5058, 1996. [arXiv:hep-th/9511071](#), [doi:10.1103/PhysRevD.54.5049](#).
- [15] Carlos A.R. Herdeiro and Eugen Radu. Asymptotically flat black holes with scalar hair: a review. *Int. J. Mod. Phys. D*, 24(09):1542014, 2015. [arXiv:1504.08209](#), [doi:10.1142/S0218271815420146](#).
- [16] Thibault Damour and Gilles Esposito-Farese. Nonperturbative strong field effects in tensor - scalar theories of gravitation. *Phys. Rev. Lett.*, 70:2220–2223, 1993. [doi:10.1103/PhysRevLett.70.2220](#).
- [17] Vitor Cardoso, Isabella P. Carucci, Paolo Pani, and Thomas P. Sotiriou. Matter around Kerr black holes in scalar-tensor theories: scalarization and superradiant instability. *Phys. Rev. D*, 88:044056, 2013. [arXiv:1305.6936](#), [doi:10.1103/PhysRevD.88.044056](#).
- [18] Vitor Cardoso, Isabella P. Carucci, Paolo Pani, and Thomas P. Sotiriou. Black holes with surrounding matter in scalar-tensor theories. *Phys. Rev. Lett.*, 111:111101, 2013. [arXiv:1308.6587](#), [doi:10.1103/PhysRevLett.111.111101](#).
- [19] Daniela D. Doneva and Stoytcho S. Yazadjiev. New Gauss-Bonnet Black Holes with Curvature-Induced Scalarization in Extended Scalar-Tensor Theories. *Phys. Rev. Lett.*, 120(13):131103,

2018. [arXiv:1711.01187](#), [doi:10.1103/PhysRevLett.120.131103](#).
- [20] Hector O. Silva, Jeremy Sakstein, Leonardo Gualtieri, Thomas P. Sotiriou, and Emanuele Berti. Spontaneous scalarization of black holes and compact stars from a Gauss-Bonnet coupling. *Phys. Rev. Lett.*, 120(13):131104, 2018. [arXiv:1711.02080](#), [doi:10.1103/PhysRevLett.120.131104](#).
- [21] G. Antoniou, A. Bakopoulos, and P. Kanti. Evasion of No-Hair Theorems and Novel Black-Hole Solutions in Gauss-Bonnet Theories. *Phys. Rev. Lett.*, 120(13):131102, 2018. [arXiv:1711.03390](#), [doi:10.1103/PhysRevLett.120.131102](#).
- [22] Daniela D. Doneva, Stella Kiorpelidi, Petya G. Nedkova, Eleftherios Papantonopoulos, and Stoytcho S. Yazadjiev. Charged Gauss-Bonnet black holes with curvature induced scalarization in the extended scalar-tensor theories. *Phys. Rev. D*, 98(10):104056, 2018. [arXiv:1809.00844](#), [doi:10.1103/PhysRevD.98.104056](#).
- [23] Pedro V.P. Cunha, Carlos A.R. Herdeiro, and Eugen Radu. Spontaneously Scalarized Kerr Black Holes in Extended Scalar-Tensor–Gauss-Bonnet Gravity. *Phys. Rev. Lett.*, 123(1):011101, 2019. [arXiv:1904.09997](#), [doi:10.1103/PhysRevLett.123.011101](#).
- [24] Carlos A. R. Herdeiro, Eugen Radu, Hector O. Silva, Thomas P. Sotiriou, and Nicolás Yunes. Spin-induced scalarized black holes. *Phys. Rev. Lett.*, 126(1):011103, 2021. [arXiv:2009.03904](#), [doi:10.1103/PhysRevLett.126.011103](#).
- [25] Carlos A.R. Herdeiro, Eugen Radu, Nicolas Sanchis-Gual, and José A. Font. Spontaneous Scalarization of Charged Black Holes. *Phys. Rev. Lett.*, 121(10):101102, 2018. [arXiv:1806.05190](#), [doi:10.1103/PhysRevLett.121.101102](#).
- [26] Pedro G.S. Fernandes, Carlos A.R. Herdeiro, Alexandre M. Pombo, Eugen Radu, and Nicolas Sanchis-Gual. Spontaneous Scalarisation of Charged Black Holes: Coupling Dependence and Dynamical Features. *Class. Quant. Grav.*, 36(13):134002, 2019. [Erratum: *Class.Quant.Grav.* 37, 049501 (2020)]. [arXiv:1902.05079](#), [doi:10.1088/1361-6382/ab23a1](#).
- [27] Jose Luis Blázquez-Salcedo, Carlos A.R. Herdeiro, Jutta Kunz, Alexandre M. Pombo, and Eugen Radu. Einstein-Maxwell-scalar black holes: the hot, the cold and the bald. *Phys. Lett. B*, 806:135493, 2020. [arXiv:2002.00963](#), [doi:10.1016/j.physletb.2020.135493](#).
- [28] D. Astefanesei, C. Herdeiro, A. Pombo, and E. Radu. Einstein-Maxwell-scalar black holes: classes of solutions, dyons and extremality. *JHEP*, 10:078, 2019. [arXiv:1905.08304](#), [doi:10.1007/JHEP10\(2019\)078](#).

- [29] Pedro G.S. Fernandes, Carlos A.R. Herdeiro, Alexandre M. Pombo, Eugen Radu, and Nicolas Sanchis-Gual. Charged black holes with axionic-type couplings: Classes of solutions and dynamical scalarization. *Phys. Rev. D*, 100(8):084045, 2019. [arXiv:1908.00037](#), [doi:10.1103/PhysRevD.100.084045](#).
- [30] De-Cheng Zou and Yun Soo Myung. Scalarized charged black holes with scalar mass term. *Phys. Rev. D*, 100(12):124055, 2019. [arXiv:1909.11859](#), [doi:10.1103/PhysRevD.100.124055](#).
- [31] Pedro G.S. Fernandes. Einstein-Maxwell-scalar black holes with massive and self-interacting scalar hair. *Phys. Dark Univ.*, 30:100716, 2020. [arXiv:2003.01045](#), [doi:10.1016/j.dark.2020.100716](#).
- [32] Yan Peng. Scalarization of horizonless reflecting stars: neutral scalar fields non-minimally coupled to Maxwell fields. *Phys. Lett. B*, 804:135372, 2020. [arXiv:1912.11989](#), [doi:10.1016/j.physletb.2020.135372](#).
- [33] Yun Soo Myung and De-Cheng Zou. Instability of Reissner–Nordström black hole in Einstein-Maxwell-scalar theory. *Eur. Phys. J. C*, 79(3):273, 2019. [arXiv:1808.02609](#), [doi:10.1140/epjc/s10052-019-6792-6](#).
- [34] Yun Soo Myung and De-Cheng Zou. Stability of scalarized charged black holes in the Einstein–Maxwell–Scalar theory. *Eur. Phys. J. C*, 79(8):641, 2019. [arXiv:1904.09864](#), [doi:10.1140/epjc/s10052-019-7176-7](#).
- [35] De-Cheng Zou and Yun Soo Myung. Radial perturbations of the scalarized black holes in Einstein-Maxwell-conformally coupled scalar theory. *Phys. Rev. D*, 102(6):064011, 2020. [arXiv:2005.06677](#), [doi:10.1103/PhysRevD.102.064011](#).
- [36] Dumitru Astefanesei, Carlos Herdeiro, João Oliveira, and Eugen Radu. Higher dimensional black hole scalarization. *JHEP*, 09:186, 2020. [arXiv:2007.04153](#), [doi:10.1007/JHEP09\(2020\)186](#).
- [37] Yun Soo Myung and De-Cheng Zou. Quasinormal modes of scalarized black holes in the Einstein–Maxwell–Scalar theory. *Phys. Lett. B*, 790:400–407, 2019. [arXiv:1812.03604](#), [doi:10.1016/j.physletb.2019.01.046](#).
- [38] Jose Luis Blázquez-Salcedo, Carlos A.R. Herdeiro, Sarah Kahlen, Jutta Kunz, Alexandre M. Pombo, and Eugen Radu. Quasinormal modes of hot, cold and bald Einstein-Maxwell-scalar black holes. 8 2020. [arXiv:2008.11744](#).

- [39] Yun Soo Myung and De-Cheng Zou. Scalarized charged black holes in the Einstein-Maxwell-Scalar theory with two U(1) fields. *Phys. Lett. B*, 811:135905, 2020. [arXiv:2009.05193](#), [doi:10.1016/j.physletb.2020.135905](#).
- [40] Yun Soo Myung and De-Cheng Zou. Scalarized black holes in the Einstein-Maxwell-scalar theory with a quasitopological term. *Phys. Rev. D*, 103(2):024010, 2021. [arXiv:2011.09665](#), [doi:10.1103/PhysRevD.103.024010](#).
- [41] R.A. Konoplya and A. Zhidenko. Analytical representation for metrics of scalarized Einstein-Maxwell black holes and their shadows. *Phys. Rev. D*, 100(4):044015, 2019. [arXiv:1907.05551](#), [doi:10.1103/PhysRevD.100.044015](#).
- [42] Shahar Hod. Spontaneous scalarization of charged Reissner-Nordström black holes: Analytic treatment along the existence line. *Phys. Lett. B*, 798:135025, 2019. [arXiv:2002.01948](#).
- [43] Shahar Hod. Reissner-Nordström black holes supporting nonminimally coupled massive scalar field configurations. *Phys. Rev. D*, 101(10):104025, 2020. [arXiv:2005.10268](#), [doi:10.1103/PhysRevD.101.104025](#).
- [44] Harald H. Soleng. Charged black points in general relativity coupled to the logarithmic U(1) gauge theory. *Phys. Rev. D*, 52:6178–6181, 1995. [arXiv:hep-th/9509033](#), [doi:10.1103/PhysRevD.52.6178](#).
- [45] Eloy Ayon-Beato and Alberto Garcia. Regular black hole in general relativity coupled to nonlinear electrodynamics. *Phys. Rev. Lett.*, 80:5056–5059, 1998. [arXiv:gr-qc/9911046](#), [doi:10.1103/PhysRevLett.80.5056](#).
- [46] Hideki Maeda, Mokhtar Hassaine, and Cristian Martinez. Lovelock black holes with a nonlinear Maxwell field. *Phys. Rev. D*, 79:044012, 2009. [arXiv:0812.2038](#), [doi:10.1103/PhysRevD.79.044012](#).
- [47] Xiaobo Guo, Peng Wang, and Haitang Yang. Membrane Paradigm and Holographic DC Conductivity for Nonlinear Electrodynamics. *Phys. Rev. D*, 98(2):026021, 2018. [arXiv:1711.03298](#), [doi:10.1103/PhysRevD.98.026021](#).
- [48] Benrong Mu, Peng Wang, and Haitang Yang. Holographic DC Conductivity for a Power-law Maxwell Field. *Eur. Phys. J. C*, 78(12):1005, 2018. [arXiv:1711.06569](#), [doi:10.1140/epjc/s10052-018-6491-8](#).
- [49] Peng Wang, Houwen Wu, and Haitang Yang. Thermodynamics and Phase Transition of a Nonlinear Electrodynamics Black Hole in a Cavity. *JHEP*, 07:002, 2019. [arXiv:1901.06216](#),

- [doi:10.1007/JHEP07\(2019\)002](https://doi.org/10.1007/JHEP07(2019)002).
- [50] Peng Wang, Houwen Wu, and Haitang Yang. Thermodynamics of nonlinear electrodynamics black holes and the validity of weak cosmic censorship at charged particle absorption. *Eur. Phys. J. C*, 79(7):572, 2019. [doi:10.1140/epjc/s10052-019-7090-z](https://doi.org/10.1140/epjc/s10052-019-7090-z).
- [51] Peng Wang, Houwen Wu, and Haitang Yang. Holographic DC Conductivity for Backreacted Nonlinear Electrodynamics with Momentum Dissipation. *Eur. Phys. J. C*, 79(1):6, 2019. [arXiv:1805.07913](https://arxiv.org/abs/1805.07913), [doi:10.1140/epjc/s10052-018-6503-8](https://doi.org/10.1140/epjc/s10052-018-6503-8).
- [52] M. Born and L. Infeld. Foundations of the new field theory. *Proc. Roy. Soc. Lond. A*, 144(852):425–451, 1934. [doi:10.1098/rspa.1934.0059](https://doi.org/10.1098/rspa.1934.0059).
- [53] Tanay Kr. Dey. Born-Infeld black holes in the presence of a cosmological constant. *Phys. Lett. B*, 595(1-4):484–490, 2004. [arXiv:hep-th/0406169](https://arxiv.org/abs/hep-th/0406169), [doi:10.1016/j.physletb.2004.06.047](https://doi.org/10.1016/j.physletb.2004.06.047).
- [54] Rong-Gen Cai, Da-Wei Pang, and Anzhong Wang. Born-Infeld black holes in (A)dS spaces. *Phys. Rev. D*, 70:124034, 2004. [arXiv:hep-th/0410158](https://arxiv.org/abs/hep-th/0410158), [doi:10.1103/PhysRevD.70.124034](https://doi.org/10.1103/PhysRevD.70.124034).
- [55] Sharmanthie Fernando and Don Krug. Charged black hole solutions in Einstein-Born-Infeld gravity with a cosmological constant. *Gen. Rel. Grav.*, 35:129–137, 2003. [arXiv:hep-th/0306120](https://arxiv.org/abs/hep-th/0306120), [doi:10.1023/A:1021315214180](https://doi.org/10.1023/A:1021315214180).
- [56] Ivan Zh. Stefanov, Stoytcho S. Yazadjiev, and Michail D. Todorov. Phases of 4D scalar-tensor black holes coupled to Born-Infeld nonlinear electrodynamics. *Mod. Phys. Lett. A*, 23:2915–2931, 2008. [arXiv:0708.4141](https://arxiv.org/abs/0708.4141), [doi:10.1142/S0217732308028351](https://doi.org/10.1142/S0217732308028351).
- [57] Rabin Banerjee, Sumit Ghosh, and Dibakar Roychowdhury. New type of phase transition in Reissner Nordström–AdS black hole and its thermodynamic geometry. *Phys. Lett. B*, 696:156–162, 2011. [arXiv:1008.2644](https://arxiv.org/abs/1008.2644), [doi:10.1016/j.physletb.2010.12.010](https://doi.org/10.1016/j.physletb.2010.12.010).
- [58] Daniela D. Doneva, Stoytcho S. Yazadjiev, Kostas D. Kokkotas, and Ivan Zh. Stefanov. Quasi-normal modes, bifurcations and non-uniqueness of charged scalar-tensor black holes. *Phys. Rev. D*, 82:064030, 2010. [arXiv:1007.1767](https://arxiv.org/abs/1007.1767), [doi:10.1103/PhysRevD.82.064030](https://doi.org/10.1103/PhysRevD.82.064030).
- [59] De-Cheng Zou, Shao-Jun Zhang, and Bin Wang. Critical behavior of Born-Infeld AdS black holes in the extended phase space thermodynamics. *Phys. Rev. D*, 89(4):044002, Feb 2014. URL: <https://link.aps.org/doi/10.1103/PhysRevD.89.044002>, [arXiv:1311.7299](https://arxiv.org/abs/1311.7299), [doi:10.1103/PhysRevD.89.044002](https://doi.org/10.1103/PhysRevD.89.044002).
- [60] Seyed Hossein Hendi, Behzad Eslam Panah, and Shahram Panahiyan. Einstein-Born-Infeld-

- Massive Gravity: adS-Black Hole Solutions and their Thermodynamical properties. *JHEP*, 11:157, 2015. [arXiv:1508.01311](#), [doi:10.1007/JHEP11\(2015\)157](#).
- [61] Xiao-Xiong Zeng, Xian-Ming Liu, and Li-Fang Li. Phase structure of the Born–Infeld–anti-de Sitter black holes probed by non-local observables. *Eur. Phys. J. C*, 76(11):616, 2016. [arXiv:1601.01160](#), [doi:10.1140/epjc/s10052-016-4463-4](#).
- [62] Shoulong Li, H. Lu, and Hao Wei. Dyonic (A)dS Black Holes in Einstein-Born-Infeld Theory in Diverse Dimensions. *JHEP*, 07:004, 2016. [arXiv:1606.02733](#), [doi:10.1007/JHEP07\(2016\)004](#).
- [63] Jun Tao, Peng Wang, and Haitang Yang. Testing holographic conjectures of complexity with Born–Infeld black holes. *Eur. Phys. J. C*, 77(12):817, 2017. [arXiv:1703.06297](#), [doi:10.1140/epjc/s10052-017-5395-3](#).
- [64] Amin Dehyadegari and Ahmad Sheykhi. Reentrant phase transition of Born-Infeld-AdS black holes. *Phys. Rev. D*, 98(2):024011, 2018. [arXiv:1711.01151](#), [doi:10.1103/PhysRevD.98.024011](#).
- [65] Peng Wang, Houwen Wu, and Haitang Yang. Thermodynamics and Phase Transitions of Nonlinear Electrodynamics Black Holes in an Extended Phase Space. *JCAP*, 04(04):052, 2019. [arXiv:1808.04506](#), [doi:10.1088/1475-7516/2019/04/052](#).
- [66] Kangkai Liang, Peng Wang, Houwen Wu, and Mingtao Yang. Phase structures and transitions of Born–Infeld black holes in a grand canonical ensemble. *Eur. Phys. J. C*, 80(3):187, 2020. [arXiv:1907.00799](#), [doi:10.1140/epjc/s10052-020-7750-z](#).
- [67] Qingyu Gan, Guangzhou Guo, Peng Wang, and Houwen Wu. Strong cosmic censorship for a scalar field in a Born-Infeld–de Sitter black hole. *Phys. Rev. D*, 100(12):124009, 2019. [arXiv:1907.04466](#), [doi:10.1103/PhysRevD.100.124009](#).
- [68] Larry Smarr. Mass formula for Kerr black holes. *Phys. Rev. Lett.*, 30:71–73, 1973. [Erratum: *Phys.Rev.Lett.* 30, 521–521 (1973)]. [doi:10.1103/PhysRevLett.30.71](#).
- [69] Masashi Kimura. A simple test for stability of black hole by S -deformation. *Class. Quant. Grav.*, 34(23):235007, 2017. [arXiv:1706.01447](#), [doi:10.1088/1361-6382/aa903f](#).